On the remote impacts of mid-Holocene Saharan vegetation on South American hydroclimate: a modelling intercomparison

Shivangi Tiwari[1], Riovie D. Ramos[2], Francesco S.R. Pausata[1], Allegra N. LeGrande[3], Michael Griffiths[2], Hugo Beltrami[4], ILana Wainer[5], Anne de Vernal[6], Daniel T. Litchmore[7], Deepak Chandan[8], W Richard Peltier[9], and Clay R Tabor[10]

[1]University of Quebec in Montreal
[2]William Paterson University
[3]NASA Goddard Institute for Space Studies and Center for Climate Systems Research
[4]St. Francis Xavier University
[5]Universidade de Sao Paulo
[6]GEOTOP-UQAM
[7]Columbia University
[8]University of Toronto
[9]Department of Physics, University of Toronto
[10]University of Connecticut

December 7, 2022

Abstract

Proxy reconstructions from the mid-Holocene (MH: 6,000 years ago) indicate an intensification of the West African Monsoon and a weakening of the South American Monsoon, primarily resulting from orbitally-driven insolation changes. However, model studies that account for MH orbital configurations and greenhouse gas concentrations can only partially reproduce these changes. Most model studies do not account for the remarkable vegetation changes that occurred during the MH, in particular over the Sahara, precluding realistic simulations of the period. Here, we study precipitation changes over northern Africa and South America using four fully coupled global climate models by accounting for the Saharan greening. Incorporating the Green Sahara amplifies orbitally-driven changes over both regions, and leads to an improvement in proxy-model agreement. Our work highlights the local and remote impacts of vegetation and the importance of considering vegetation changes in the Sahara when studying and modelling global climate.

On the remote impacts of mid-Holocene Saharan vegetation on South American hydroclimate: a modelling intercomparison

S. Tiwari[1], R. D. Ramos[2], F. S. R. Pausata[1], A. N. LeGrande[3,4], M. L. Griffiths[2], H. Beltrami[5], I. Wainer[6], A. de Vernal[1], D. T. Litchmore[4,3], D. Chandan[7], W. R. Peltier[7], and C. R. Tabor[8]

[1]Centre ESCER (Étude et la Simulation du Climat à l'Échelle Régionale) and GEOTOP (Research Center on the dynamics of the Earth System), Department of Earth and Atmospheric Sciences, University of Quebec in Montreal, Montreal, Canada.
[2]Department of Environmental Science, William Paterson University, Wayne, New Jersey, USA.
[3]NASA Goddard Institute for Space Studies, New York, New York, USA.
[4]Center for Climate Systems Research, Columbia University, New York, New York, USA.
[5]Department of Earth Sciences, St. Francis Xavier University, Antigonish, Nova Scotia, Canada.
[6]Departamento de Oceanografia Física, Química e Geológica, Instituto Oceanográfico da Universidade de São Paulo, Praça do Oceanográfico, Sao Paulo, Brazil.
[7]Department of Physics, University of Toronto, Toronto, Ontario, Canada.
[8]Department of Geosciences, University of Connecticut, Storrs, Connecticut, USA.

Corresponding author: Shivangi Tiwari (tiwari.shivangi@courrier.uqam.ca)

Key Points:

- We simulate the mid-Holocene with and without the Green Sahara using four fully coupled global climate models
- The mid-Holocene simulation with the Green Sahara shows intensification of orbitally-driven changes in precipitation over northern Africa and South America
- Incorporation of the Green Sahara leads to greater proxy-model agreement over both northern Africa and South America

Abstract

Proxy reconstructions from the mid-Holocene (MH: 6,000 years ago) indicate an intensification of the West African Monsoon and a weakening of the South American Monsoon, primarily resulting from orbitally-driven insolation changes. However, model studies that account for MH orbital configurations and greenhouse gas concentrations can only partially reproduce these changes. Most model studies do not account for the remarkable vegetation changes that occurred during the MH, in particular over the Sahara, precluding realistic simulations of the period. Here, we study precipitation changes over northern Africa and South America using four fully coupled global climate models by accounting for the Saharan greening. Incorporating the Green Sahara amplifies orbitally-driven changes over both regions, and leads to an improvement in proxy-model agreement. Our work highlights the local and remote impacts of vegetation and the importance of considering vegetation changes in the Sahara when studying and modelling global climate.

Plain Language Summary

Paleoclimate modelling offers a way to test the ability of climate models to detect climate change outside the envelope of historical climatic variability. The mid-Holocene (MH: 6,000 years ago) is a key interval for paleoclimate studies, as the Northern Hemisphere received greater summer-time insolation and experienced stronger monsoons than today. Due to a stronger MH West African Monsoon, the Saharan region received enough rainfall to be able to host vegetation. The vegetation changes in the Sahara affected not only the local climate but also far-afield locations through teleconnections in the global climate system. In this study, we simulate the MH climate using four climate models, each with two types of simulations – with and without the Green Sahara. We show that simulations with the Green Sahara capture greater drying over the South American continent than the simulations which only account for changes in orbital forcing and greenhouse gas concentrations. The simulations with the Green Sahara are more in line with proxy reconstructions, lending further support to incorporating vegetation changes as a necessary boundary condition to simulate the MH climate realistically.

1 Introduction

Vegetation cover is known to impact regional climate variability, but the magnitude and global implications of vegetation changes are not well constrained due to the limited variability over the historical period. The Paleoclimate Modelling Intercomparison Project (PMIP) coordinates experiments to determine consistent responses across models that, when constrained against proxy reconstructions, can provide for a deeper understanding of how the climate system operates (Braconnot et al., 2012; Otto-Bliesner et al., 2017; Kageyama et al., 2018). A key interval for study is the mid-Holocene (MH), which refers to the time-slice around 6,000 years ago. The MH was characterized by paleogeographic and ice-sheet distributions comparable to today, but the orbital configuration and greenhouse gas (GHG) composition differed. Most notably, the perihelion occurred during boreal autumn as opposed to boreal winter today, enhancing Northern Hemisphere seasonality. The Northern (Southern) Hemisphere received greater (lesser) summer insolation relative to the present day. In addition, carbon dioxide and methane compositions were lower by ~7% and ~26% respectively, relative to the pre-industrial (PI) period (Otto-Bliesner et al., 2017). These differences are prescribed in the coordinated PMIP4 *midHolocene* experiments. The PMIP4 MH simulations indicate stronger monsoons in the Northern Hemisphere, especially over northern Africa (Brierley et al., 2020). This is supported by multi-proxy reconstructions from various archives such as organic biomarkers (Shanahan et al., 2015; Collins et al., 2017; Tierney et al., 2017), dust (McGee et al., 2013; Palchan et al., 2019), pollen (Bartlein et al., 2011; Hély et al., 2014), speleothems (Sha et al., 2019) and paleohydrological records (Gasse et al., 2000; Lézine et al., 2011). However, proxy-model comparisons indicate that climate models generally under-estimate the magnitude of African precipitation change with too little rainfall to support the proxy reconstructed vegetation (Braconnot et al., 2012; Tierney et al., 2017; Brierley et al., 2020).

The proxy-model discrepancy over northern Africa may be resolved to great extent through the incorporation of appropriate vegetation in climate models. There is considerable evidence that there were large-scale vegetation changes throughout the world during the MH (Bartlein et al., 2011). Most notably, the expansion of grasslands and shrubs into the current desert region of the Sahara (the so-called "Green Sahara"; e.g., Hély et al., 2014) led to significant amplification of the orbital-driven strengthening of the West African Monsoon (WAM) through positive non-linear feedbacks such as vegetation, dust and albedo feedbacks (Swann et al., 2014; Pausata et al., 2020). The incorporation of these changes, either through dynamic vegetation (e.g., Levis et al., 2004; Rachmayani et al. 2015; Dallmeyer et al., 2021) or through the prescription of vegetation distributions (e.g., Pausata et al., 2016; Chandan and Peltier, 2020, Thompson et al., 2021), leads to simulations that are more consistent with proxy reconstructions. An important consequence of more realistic simulations is the enhanced ability to identify the far-afield impacts of the Green Sahara. For example, simulations accounting for the MH Green Sahara have elucidated the influence of the WAM on the El-Niño Southern Oscillation (Pausata et al., 2017a), tropical cyclone activity (Pausata et al., 2017b), global monsoon systems (Sun et al., 2019; Griffiths et al., 2020; Piao et al., 2020; Tabor et al., 2020, Huo et al., 2021) and high latitude climate (Muschitiello et al., 2015). While the regional changes that accompanied the Green Sahara are well-recognized, its remote impacts warrant further exploration.

The MH WAM intensification occurred in parallel with a reduction in precipitation over parts of South America. Proxy reconstructions from pollen, sedimentological and isotopic records indicate that a drier MH climate prevailed over most of tropical South America (Baker et al., 2001; Cruz et al., 2005; Novello et al., 2017; see Gorenstein et al., 2022 for a synthesis); some exceptions are found from the Cariaco Basin (Haug et al., 2001), northeast Brazil (Cruz et al., 2009) and western Amazonia (Wang et al., 2017). While PMIP4 models in general capture this reduction in precipitation (Brierley and Wainer, 2018; Brierley et al., 2020), closer inspection reveals less consistency amongst them regarding the reduction in South American precipitation, compared with northern Africa where the models display better agreement (Brierley et al., 2020).

The South American Monsoon System (SAMS) brings precipitation during austral summer over the region extending from southern Amazon to southeastern Brazil (Garreaud et al., 2009). The MH drying over South America has been attributed primarily to lower summer insolation and dampened seasonality in the Southern Hemisphere, which led to a weakening of the SAMS. However, few studies have addressed the mechanisms by which the Green Sahara could have impacted South American climate. Dias et al. (2009) studied the effect of vegetation changes with two MH experiments: the first considered changes only in orbital parameters, the second additionally incorporated vegetation changes by asynchronously coupling a vegetation model to an ocean-atmosphere climate model. They observed that vegetation feedbacks could enhance some orbitally driven patterns, especially the displacement of the Intertropical Convergence Zone (ITCZ). Recently, Tabor et al. (2020) used a water isotope-enabled Earth System Model to simulate $d^{18}O$ changes during the MH and compare them with speleothem reconstructions. They found that the incorporation of the Green Sahara led to better proxy-model agreement with the amplification of the drying signal over South America.

Therefore, tropical African vegetation changes are a critical prerequisite for a realistic simulation of MH climate, as well as for the identification of the remote impacts of the Green Sahara. In this study, we investigate the response of the climate of northern African and South America to the incorporation of a Green Sahara. To this end, we examine the differences between two MH simulations – with and without the Green Sahara – based on simulations from four coupled global climate models. To the best of our knowledge, this is the first model intercomparison study regarding the effects of land surface changes due to the Green Sahara. We also present a semi-quantitative assessment of the improved proxy-model agreement upon the inclusion of the Green Sahara, which lends further support to our approach.

2 Methods

2.1 Climate models and experiments

For this study, we analyzed outputs from four global climate models – (i) EC-Earth version 3.1 (Hazeleger et al., 2010), (ii) the water isotope-enabled Community Earth System Model version 1.2 (iCESM1; Brady et al., 2019), (iii) University of Toronto version of CCSM4 (hereby referred to as UofT-CCSM4; Peltier and Vettoretti, 2014) and (iv) the water isotope-enabled GISS-E2.1-G (Kelley et al., 2020). Details about the atmospheric and oceanic components of these models and their associated grids are provided in Table S1. Three simulations were analyzed for each model – one for the pre-industrial (PI) and two for the mid-Holocene (MH) climate state. The first MH experiment follows the standard forcings and boundary conditions as specified by the PMIP4 guidelines (Otto-Bliesner et al., 2017) and is referred to as MH_{PMIP}. These guidelines comprise changes to orbital parameters and greenhouse gas concentrations. The second MH simulation, which additionally incorporates a Green Sahara by prescribing vegetation over northern Africa, is referred to as the MH_{GS}. While the representation of the Green Sahara is different in each climate model, it broadly follows the paleodistributions of vegetation suggested for the PMIP4 sensitivity experiments (Otto-Bliesner et al., 2017). The vegetation change leads to a reduction in surface albedo from ~0.3 to 0.15-0.19 over the Sahara. Further details about the representation of the Green Sahara in the MH_{GS} experiment in the different models is provided in the Supplementary Text S1.

To validate the models, we compared climatological outputs from PI simulations with the Global Precipitation Climatology Centre (GPCC) Reanalysis Dataset from 1951-80 (Schneider et al., 2011) and the Global Precipitation Climatology Project (GPCP) dataset v2.2 from 1979-2009 (Huffman et al., 2015) (Text S1 and Fig. S2). The models broadly reproduce the magnitudes and distributions of annual precipitation over the study area. iCESM 1.2 shows a dry bias over northwestern South America (~2 mm/day). Notwithstanding some local precipitation hotspots, GISS-E2.1-G shows a dry bias over the domain of the SAMS (which extends from southern

Amazon to southeastern Brazil), as well as over the Sahel. To redress the effect of model biases, we discuss our results in terms of MH – PI differences. Only differences significant at the 95% confidence level are shown. We interpret the MH_{PMIP} - PI anomalies to reflect the effects of changes in orbital parameters and greenhouse gas concentrations, and the MH_{GS} - MH_{PMIP} anomalies to reflect the additional effect of the Green Sahara. All model climate variables are analyzed as averages over 100 simulation years.

2.2 Precipitation proxies

To compare the effects of the Green Sahara on monsoon regimes within northern Africa and South America, we considered precipitation proxies from terrestrial and marine records within these respective domains: 0°-38°N; 20°W-45°E and 50°S-15°N; 80°W-30°W. The proxy data, derived from previously synthesized databases, includes records of pollen-based mean annual precipitation reconstructions (Bartlein *et al.*, 2011), lake level records from Africa (Tierney *et al.*, 2011), and an updated multiproxy hydroclimate reconstruction from South America (Gorenstein *et al.*, 2022). We also included hydroclimate reconstructions from Bolivia, Colombia and Peru (Harrison *et al.*, 2003) to fill in more data gaps in the tropical South American region. In total, we have collated 252 proxy records in which each MH hydroclimate response relative to PI is compared against model outputs.

2.3 Proxy-model comparison

To compare the proxies with models, MH precipitation responses relative to PI conditions were all categorically defined as either drier (rated as -1), wetter (1), or unchanged (0). Field reconstructions of mean annual precipitation from (Bartlein *et al.*, 2011) were converted to these categories based on the reported change for each grid point. Original classifications of lake level reconstructions from Africa (i.e., "low", "intermediate", and "high" (Tierney *et al.*, 2011)) for MH and PI periods were used to derive lake level status. These included higher, lower and unchanged to represent wetter, drier and unchanged, respectively. Categories for hydroclimate reconstructions from South America and additional records in this region follow the interpretation of the original publications (i.e., Harrison *et al.*, 2003; Gorenstein *et al.*, 2022). Simulated changes in precipitation from the nearest grid points to the proxy sites were extracted and similarly placed into three categories based on the direction of change and statistical significance.

To quantify the agreement between models and proxies, we used Cohen's κ statistic defined as the observed fractional agreement (p_o) between raters (i.e., proxies and models) relative to the probability of random agreement (p_e):

$$\mathrm{k} = \frac{p_o - p_e}{1 - p_e};$$

where p_o is the sum of the diagonal elements in the proxy-model matrix divided by the total number of samples, *N*; and p_e is the product of the sum of each matrix row and column (given by the frequency of occurrence of each category) normalized by *N*. We implemented weights in the κ calculation by multiplying the data by a weight matrix that penalizes models for a total disagreement (i.e., drier when it should be wetter and vice versa) to a value of 0 and near miss (i.e., drier or wetter when it should be unchanged) to a value of 0.5.

3 Results

The MH_{PMIP} simulations indicate a small but significant increase in precipitation of 0.5 mm/day over almost the entirety of northern Africa, extending beyond 30 °N (Fig. 1, a-d). The intensification of the WAM is larger over the Sahel, where it reaches the order of 1-2 mm/day between the equator and 15 °N and is also reflected in stronger low-level (850 hPa) southwesterly monsoon winds. An increase of 0.5 mm/day and 2 mm/day is consistent with the northward expansion of Sahelian and Sudanian vegetation into the Sahara and the Sahel respectively, as indicated by pollen records (Hély et al., 2014). The patterns and magnitude of the increase in mean annual precipitation over northern Africa are consistent across all four models. EC-Earth 3.1 shows the highest increase of 2 mm/day over the core rainfall belt. The intensification of the WAM in the MH_{PMIP} simulations is accompanied by a decrease in mean annual precipitation over some regions of South America. This decrease is on the order of 0.5-2 mm/day but the spatial extent of the change differs among the models. EC-Earth 3.1 and GISS-E2.1-G capture a widespread decrease across nearly the full meridional extent of the continent. The UofT-CCSM4 simulation shows a greater decrease, but limited to parts of northwestern Amazon, while iCESM 1.2 shows a modest decrease of up to 0.5 mm/day in the southern half of the continent. All models show a decrease in precipitation just north of the equator in the Atlantic Ocean.

Comparing the MH_{PMIP} (Fig. 1, a-d) and the MH_{GS} (Fig. 1, e-h) simulations, we observe an amplification of orbitally-driven changes in rainfall. The increase in precipitation over northern Africa is intensified and extends further north, with three out of four models showing an increase of 0.5-1 mm/day up to 25 °N. The core rainfall belt is between 10-20 °N, with an increase in precipitation in the order of 1-3 mm/day. EC-Earth 3.1 shows the greatest increase in the core rainfall belt, exceeding 4 mm/day between 12-16 °N. This is consistent with the northward expansion of tropical Guineo-Congolian vegetation, in addition to the changes in Sahelian and Sudanian vegetation extents (Hély et al., 2014). Across the Atlantic, all models suggest greater and more widespread drying of up to 2 mm/day over South America. The drying patterns appear stronger over northern South America, but more consistent over southern South America. Notably, iCESM 1.2 shows little change from the PI over northwestern South America, with a modest but significant increase in some parts of the Amazon. All models show a decrease in precipitation immediately north of the equator and an intensification in precipitation northwards of this region, suggesting a northward shift in the position of the ITCZ. None of the MH simulations indicate an increase in precipitation over northeastern Brazil.

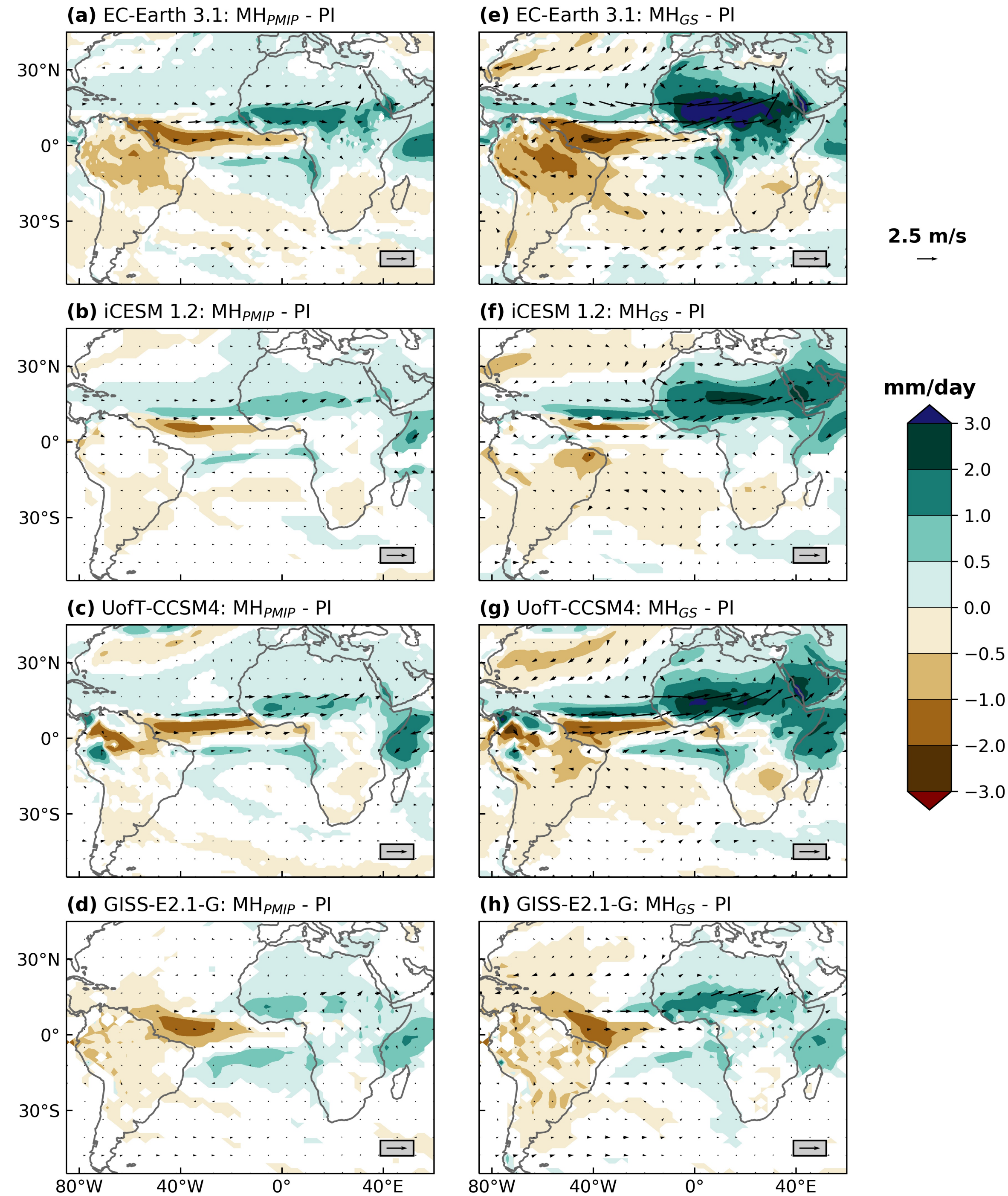

Figure 1. Change in annual precipitation in the $\mathrm{MH_{PMIP}}$ (a-d) and $\mathrm{MH_{GS}}$ (e-f) experiment relative to the PI simulation. Colors represent precipitation change in mm/day. Only changes significant at the 95% confidence level are shaded. Vectors indicate changes in low-level (850 hPa) wind strength.

As the WAM and the SAMS operate over different seasons and different regions in South America experience different annual precipitation cycles (Fig. S1), it is helpful to investigate MH-PI anomalies in monthly precipitation. The multi-model mean rainfall changes in the MH_{PMIP} simulation relative to the PI indicate an intensification of the WAM from May-October (Fig. S3). With the exception of austral spring (October-November), the dominant change observed over South America is a drying throughout the year. During austral winter (May-July), this drying is restricted to regions north of 10 °S, which are dominantly influenced by the ITCZ. The multi-model mean change in the MH_{GS} relative to PI indicate that the increase in precipitation over northern Africa lasted longer, from March-November, with a very prominent increase over the core rainfall belt around 15 °N from May-October (Fig. S4). Two notable patterns are observed in the MH_{GS} simulation relative to the PI: firstly, except for November, the domain of the SAMS was drier throughout the year; secondly, the ITCZ-influenced regions in northern South America were wetter between January-May and drier through the rest of the year. Changes in annual average values aggregate some of these seasonal changes and result in a weaker drying signal in the MH_{PMIP} simulation relative to the PI. However, since the drying signal is stronger, more widespread, and extended to a longer duration through the year in the MH_{GS} simulation relative to the PI, it remains evident in the annual average as well (Fig. 1).

The effects of incorporating the Sahara greening into the models are evident in the multi-model mean anomalies between MH_{GS} and MH_{PMIP} (Fig. 2). The Sahara greening leads to higher precipitation over northern South America between December-May, but drying over other regions throughout the year. Notably, the Green Sahara leads to a larger amplitude of precipitation seasonality in the equatorial areas such as the northern Amazon. This is because the expansion of the seasonal migration range of the ITCZ in the MH_{GS} scenario leads to an increase in precipitation over equatorial South America during austral summer and a decrease during the boreal summer. Lastly, the Saharan vegetation changes are associated with drying over northeastern Brazil throughout the year.

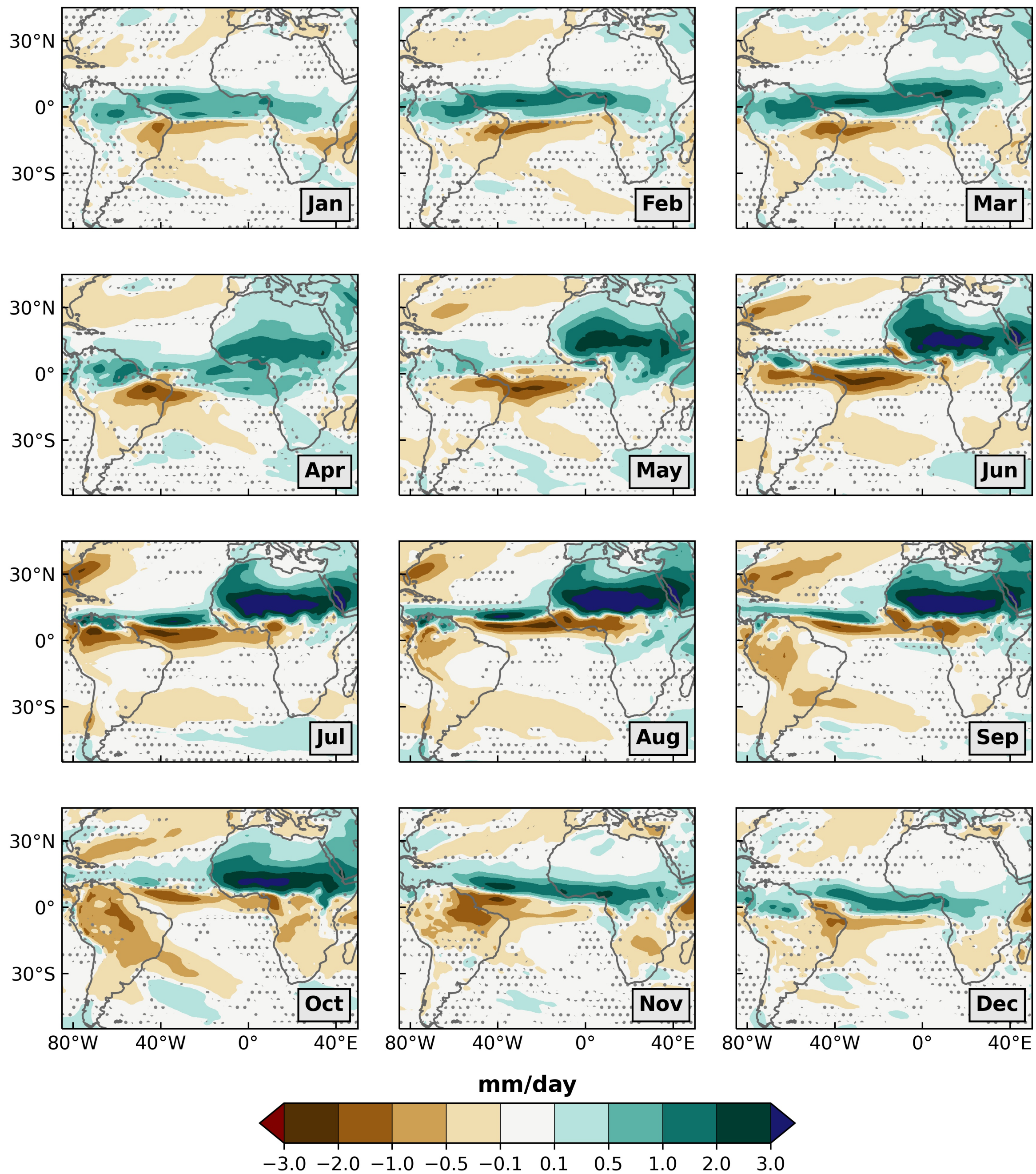

Figure 2. Monthly evolution of the multi-model average precipitation anomalies between MH_{GS} and MH_{PMIP}. Areas in which less than three models agree on the sign change are hatched.

We assessed the agreement between proxies and models under different MH experiments using weighted Cohen's κ statistic, a semi-quantitative metric to estimate the frequency of agreement between categorical data. All models show higher κ scores in the MH_{GS} (i.e., $\kappa > 0.49$, $p < 0.01$) compared to MH_{PMIP} (i.e., $\kappa < 0.48$, $p < 0.01$) experiment, with EC-Earth 3.1 and iCESM 1.2

showing the most significant improvements (Fig. 3; Fig. S5a; Fig. S6). This indicates that the MH_{GS} simulation better simulates the extent of a wetter northern Africa and/or a drier South America during this period relative to the MH_{PMIP} simulation. Considering the proxy-model agreement between the continents, northern Africa consistently shows higher κ scores than South America (Fig. S5b and S5c) with all models showing a general improvement in reflecting a greener Sahara. Over South America, all models except for GISS-E2.1-G show an improvement in capturing the drier conditions in this region in the MH_{GS} experiment (Fig. S5c). UofT-CCSM4 performed well over northern Africa but worse over South America resulting in overall comparable κ scores between MH scenarios (Fig. 3; Fig. S5). For GISS-E2.1-G, the κ score over South America decreases but there is a general improvement over northern Africa in the MH_{GS} simulation with comparable κ scores between MH experiments (Fig. 3; Fig. S5). The observed overall improvement in iCESM 1.2 originates from the more apparent drying over South America under MH_{GS} relative to MH_{PMIP} (Fig. 1). EC-Earth 3.1 shows the highest κ score for both continents, outperforming all models under MH_{GS} scenarios (Fig. S5).

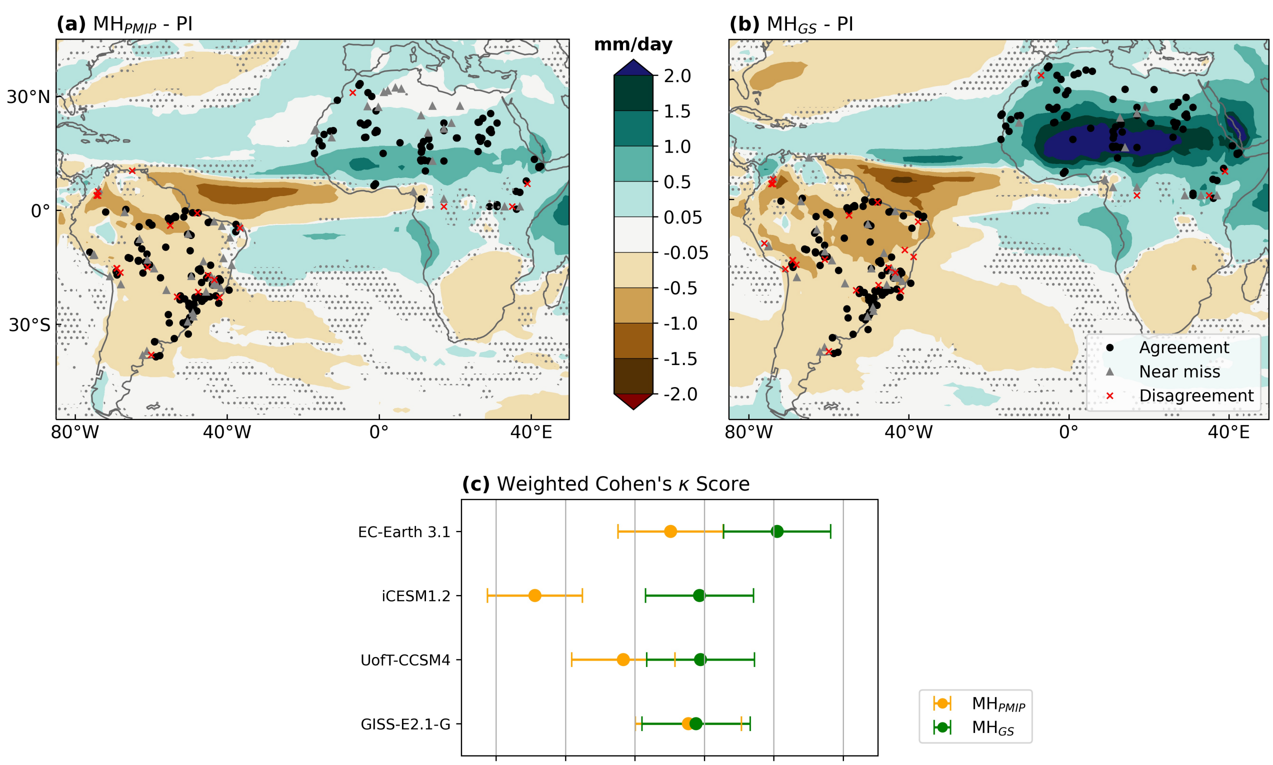

Figure. 3. Multi-model mean change in annual precipitation, with proxy-model agreement overlain. Colors indicate (a) MH_{PMIP} – PI and (b) MH_{GS} – PI changes in annual precipitation in mm/day. Areas in which less than three models agree on the sign change are hatched. Proxy-model agreement is indicated as agreement (black circles), near miss (grey triangles) or disagreement (red crosses). (c) Weighted Cohen's κ Scores for MH_{PMIP} (orange symbols) and MH_{GS} (green symbols) runs. Error bars indicate 95% confidence intervals.

4 Discussion and Conclusions

In this study, we studied the impact of paleovegetation changes during the MH by considering two simulations – with and without the Green Sahara. A model intercomparison to robustly assess the northern African land cover changes was hitherto missing. For the first time, we compare four different Earth system models in which vegetation changes over northern Africa are account for, and focus on the associated hydroclimate changes over northern Africa and South America. Irrespective of the methods used to prescribe vegetation, the models share similarities in their teleconnections across the tropical and extra-tropical Atlantic. Thus, while different models include different aspects of the Green Sahara-modulated climate impact through varying vegetation, dust, soil and lake modifications, they show similar responses, owing to the overwhelming importance of these vegetation changes. The Sahara greening (MH_{GS}) enhances the rainfall over northern Africa, while further decreasing precipitation over South America relative to the case in which only orbital forcing are accounted for (MH_{PMIP}).

Several modelling studies have shown a reduction in precipitation over South America as well as changes to the monsoonal cycle due to changes in seasonal insolation (Shimizu et al., 2021). The orbital-driven weakening of the SAMS during austral summer is indicated by PMIP3 (Prado et al., 2013, Shimizu et al., 2020) as well as PMIP4 models (Brierley et al., 2020). Our MH_{PMIP} simulations similarly capture a drying signal, particularly over northwestern South America (Fig. 1) and provide drying estimates comparable to previous results (around 1 mm/day). Examining the seasonal cycle indicates that South America received less insolation during austral summer and more insolation during austral spring during the mid-Holocene compared with the PI, which could have altered the cycle of the SAM (Shimizu et al., 2020). Our MH_{PMIP} simulations also capture these changes through a decrease in precipitation over the SAMS region during December-February, but an increase during October-November. However, few of the previous modelling studies focused specifically on how the Sahara greening may have influenced the MH South American hydroclimate (Dias et al., 2009; Tabor et al., 2020). Our results support their findings regarding the impact of the Green Sahara in amplifying orbital-driven weakening of the SAMS, through consistent results from four different models. Furthermore, in our study we show that South America also experienced a significant reduction in precipitation during austral winter, most likely because the prescribed vegetation led to widespread moisture redistribution during austral winter (Fig. 2). Combined with a weakening of the SAMS during austral summer, this led to longer and greater drying over South America than seen when only considering changes in orbital forcings. Thus, the drying in South America during the MH was prevalent throughout the year and not exclusively related to changes in the SAMS.

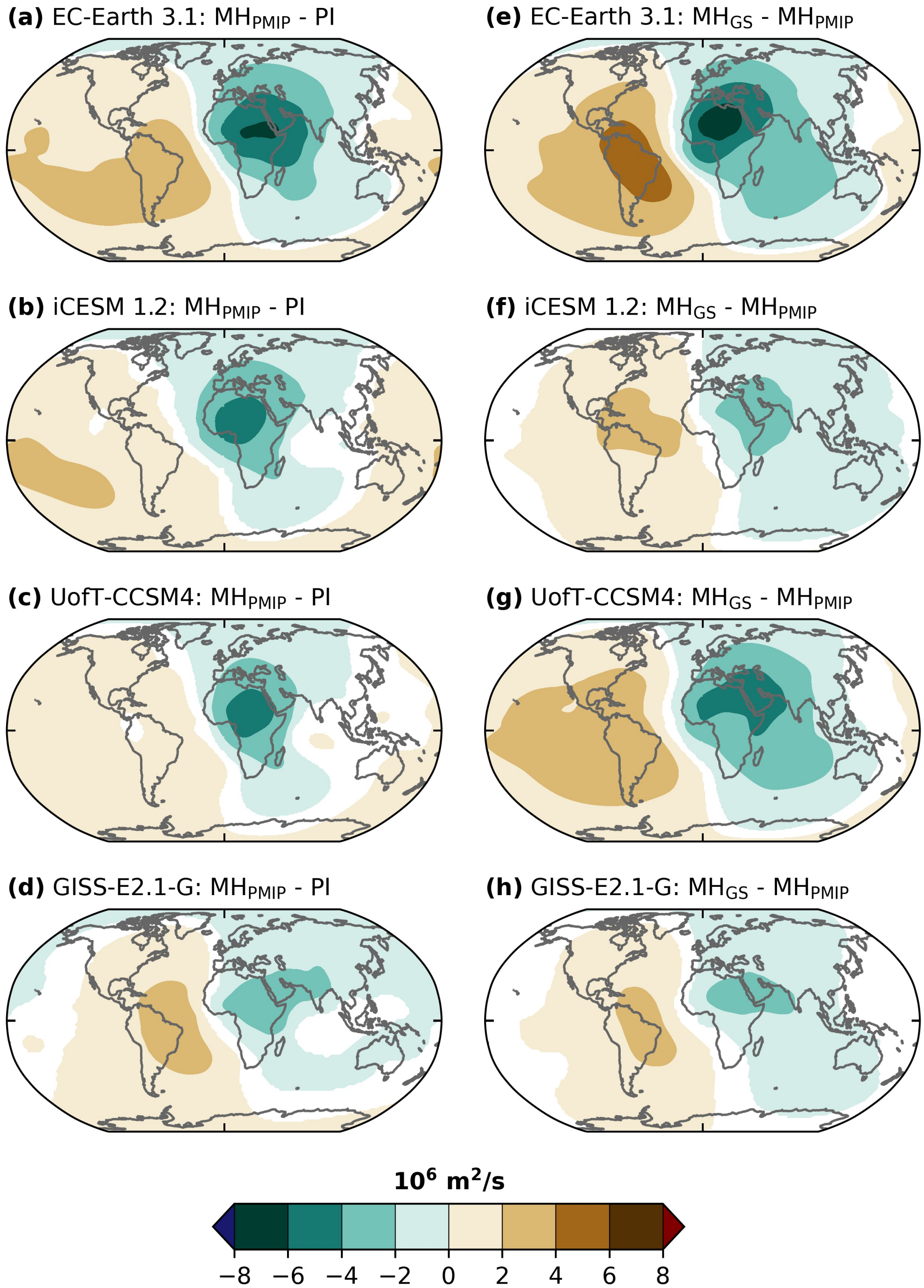

Figure 4. Changes in boreal summer (JJAS) upper-level (200 hPa) velocity potential (a-d) for the MH_{PMIP} relative to the PI experiment and (e-h) for the MH_{GS} relative to the MH_{PMIP} simulation. Only changes significant at the 95% confidence level are shaded.

Various mechanisms have been proposed to explain the influence of northern African vegetation changes on South American hydroclimate. Dias et al. (2009) suggested a northward migration of the SACZ associated with a weakening of the upper-level Bolivian High and a weakened tropical circulation. Tabor et al. (2020) discussed the role of substantial regional warming due to a Green Sahara, which acted to counteract the effects of increased insolation in the Southern Hemisphere in pulling the ITCZ southwards between November and March. The precipitation over South America was likely also modulated by changes in the equatorial Atlantic (Brierley and Wainer, 2018) and the equatorial Pacific variability (Pausata et al., 2017). While an in-depth investigation of the mechanism(s) behind the Green Sahara's modulation of South American hydroclimate is beyond the scope of this study, our work nonetheless shows the importance of Saharan vegetation in more accurately simulating northern African and South American teleconnections during the MH. This is even clearer through an analysis of boreal summer (JJAS) atmospheric circulation, namely upper-level (200 hPa) velocity potential (Fig. 4). A comparison of MH_{PMIP} - PI and MH_{GS} - MH_{PMIP} anomalies shows that the impact of the Green Sahara is comparable to the impact of the changes in orbital configuration and GHG concentrations (Fig. 4). An inadequate representation of the substantial forcing imposed by the Saharan vegetation precludes an analysis of its remote impacts.

The inclusion of vegetation changes over northern Africa in the models (MH_{GS} experiments) also leads to an overall improvement in proxy-model agreement for all models over northern Africa and South America relative to the case in which only orbital forcing are accounted for (MH_{PMIP}). In particular, EC-Earth 3.1 and iCESM 1.2, show significant improvements in model skill as benchmarked against the proxies in the MH_{GS} relative to the MH_{PMIP} experiments. On the other hand, the UofT-CCSM4 and GISS-E2.1-G results show comparable scores between the MH_{GS} and the MH_{PMIP} simulations. This is likely due to the fact that our calculations take into consideration the improvement in proxy-model agreement concerning extent, but not the magnitude of climatic changes. Notwithstanding these limitations, our work highlights the importance of vegetation as key boundary condition that should be included when simulating MH climate and comparing models to paleoclimate archives.

Acknowledgments

S.T. and F.S.R.P. acknowledge the financial support from the Natural Sciences and Engineering Research Council of Canada (grant RGPIN-2018-04981) and the Fonds de recherche du Québec–Nature et technologies (2020-NC-268559). S. T. has been partially supported by the Canada Research Chairs Program (grant no. CRC 230687) and the Natural Sciences and Engineering Research Council (grant no. NSERC DG 140576948). A. N. L. thanks NASA GISS and NASA NCCS for institutional support. This research was supported by a National Science Foundation Paleo Perspectives on Climate Change (P2C2) grant (Award #2202999) to M.L.G.

Open Research

All data presented here are accessible from the Zenodo repository:
https://doi.org/10.5281/zenodo.7274836
This repository contains the model outputs as well as Python scripts that can be used to reproduce the figures discussed in this article.

References

Baker, P. A., Rigsby, C. A., Seltzer, G. O., Fritz, S. C., Lowenstein, T. K., Bacher, N. P., & Veliz, C. (2001). Tropical climate changes at millennial and orbital timescales on the Bolivian Altiplano. *Nature*, *409*(6821), 698-701.

Bartlein, P. J., Harrison, S. P., Brewer, S., Connor, S., Davis, B. A. S., Gajewski, K., ... & Wu, H. (2011). Pollen-based continental climate reconstructions at 6 and 21 ka: a global synthesis. *Climate Dynamics*, *37*(3), 775-802.

Braconnot, P., Joussaume, S., De Noblet, N., & Ramstein, G. (2000). Mid-Holocene and last glacial maximum African monsoon changes as simulated within the paleoclimate modelling intercomparison project. *Global and planetary change*, *26*(1-3), 51-66.

Braconnot, P., Harrison, S. P., Kageyama, M., Bartlein, P. J., Masson-Delmotte, V., Abe-Ouchi, A., ... & Zhao, Y. (2012). Evaluation of climate models using palaeoclimatic data. *Nature Climate Change*, *2*(6), 417-424.

Brady, E., Stevenson, S., Bailey, D., Liu, Z., Noone, D., Nusbaumer, J., ... & Zhu, J. (2019). The connected isotopic water cycle in the Community Earth System Model version 1. *Journal of Advances in Modeling Earth Systems*, *11*(8), 2547-2566.

Brierley, C., & Wainer, I. (2018). Inter-annual variability in the tropical Atlantic from the Last Glacial Maximum into future climate projections simulated by CMIP5/PMIP3. *Climate of the Past*, *14*(10), 1377-1390.

Brierley, C. M., Zhao, A., Harrison, S. P., Braconnot, P., Williams, C. J., Thornalley, D. J., ... & Abe-Ouchi, A. (2020). Large-scale features and evaluation of the PMIP4-CMIP6 midHolocene simulations. *Climate of the Past*, *16*(5), 1847-1872.

Chandan, D., & Peltier, W. R. (2020). African humid period precipitation sustained by robust vegetation, soil, and Lake feedbacks. *Geophysical Research Letters*, *47*(21), e2020GL088728.

Collins, J. A., Prange, M., Caley, T., Gimeno, L., Beckmann, B., Mulitza, S., ... & Schefuß, E. (2017). Rapid termination of the African Humid Period triggered by northern high-latitude cooling. *Nature communications*, *8*(1), 1-11.

Cruz, F. W., Burns, S. J., Karmann, I., Sharp, W. D., Vuille, M., Cardoso, A. O., ... & Viana, O. (2005). Insolation-driven changes in atmospheric circulation over the past 116,000 years in subtropical Brazil. *Nature*, *434*(7029), 63-66.

Cruz, F. W., Vuille, M., Burns, S. J., Wang, X., Cheng, H., Werner, M., ... & Nguyen, H. (2009). Orbitally driven east–west antiphasing of South American precipitation. *Nature Geoscience*, *2*(3), 210-214.

Dallmeyer, A., Claussen, M., Lorenz, S. J., Sigl, M., Toohey, M., & Herzschuh, U. (2021). Holocene vegetation transitions and their climatic drivers in MPI-ESM1. 2. *Climate of the Past*, *17*(6), 2481-2513.

Gasse, F. (2000). Hydrological changes in the African tropics since the Last Glacial Maximum. *Quaternary Science Reviews*, *19*(1-5), 189-211.

Gorenstein, I., Prado, L. F., Bianchini, P. R., Wainer, I., Griffiths, M. L., Pausata, F. S., & Yokoyama, E. (2022). A fully calibrated and updated mid-Holocene climate reconstruction for Eastern South America. *Quaternary Science Reviews*, *292*, 107646.

Griffiths, M. L., Johnson, K. R., Pausata, F. S., White, J. C., Henderson, G. M., Wood, C. T., ... & Sekhon, N. (2020). End of Green Sahara amplified mid-to late Holocene megadroughts in mainland Southeast Asia. *Nature communications*, *11*(1), 1-12.

Harrison, S. P. A., Kutzbach, J. E., Liu, Z., Bartlein, P. J., Otto-Bliesner, B., Muhs, D., ... & Thompson, R. S. (2003). Mid-Holocene climates of the Americas: a dynamical response to changed seasonality. *Climate Dynamics*, *20*(7), 663-688.

Haug, G. H., Hughen, K. A., Sigman, D. M., Peterson, L. C., & Rohl, U. (2001). Southward migration of the intertropical convergence zone through the Holocene. *Science*, *293*(5533), 1304-1308.

Hazeleger, W., Severijns, C., Semmler, T., Ştefănescu, S., Yang, S., Wang, X., ... & Willén, U. (2010). EC-Earth: a seamless earth-system prediction approach in action. *Bulletin of the American Meteorological Society*, *91*(10), 1357-1364.

Hély, C., & Lézine, A. M. (2014). Holocene changes in African vegetation: Tradeoff between climate and water availability. *Climate of the Past*, *10*(2), 681-686.

Hopcroft, P. O., & Valdes, P. J. (2021). Paleoclimate-conditioning reveals a North Africa land–atmosphere tipping point. *Proceedings of the National Academy of Sciences*, *118*(45), e2108783118.

Huo, Y., Peltier, W. R., & Chandan, D. (2021). Mid-Holocene monsoons in South and Southeast Asia: dynamically downscaled simulations and the influence of the Green Sahara. *Climate of the Past*, *17*(4), 1645-1664.

Kageyama, M., Braconnot, P., Harrison, S. P., Haywood, A. M., Jungclaus, J. H., Otto-Bliesner, B. L., ... & Zhou, T. (2018). The PMIP4 contribution to CMIP6–Part 1: Overview and over-arching analysis plan. *Geoscientific Model Development*, *11*(3), 1033-1057.

Kelley, M., Schmidt, G. A., Nazarenko, L. S., Bauer, S. E., Ruedy, R., Russell, G. L., ... & Yao, M. S. (2020). GISS-E2. 1: Configurations and climatology. *Journal of Advances in Modeling Earth Systems*, *12*(8), e2019MS002025.

Levis, S., Bonan, G. B., & Bonfils, C. (2004). Soil feedback drives the mid-Holocene North African monsoon northward in fully coupled CCSM2 simulations with a dynamic vegetation model. *Climate Dynamics*, *23*(7), 791-802.

Lézine, A. M., Hély, C., Grenier, C., Braconnot, P., & Krinner, G. (2011). Sahara and Sahel vulnerability to climate changes, lessons from Holocene hydrological data. *Quaternary Science Reviews*, *30*(21-22), 3001-3012.

McGee, D., deMenocal, P. B., Winckler, G., Stuut, J. B. W., & Bradtmiller, L. I. (2013). The magnitude, timing and abruptness of changes in North African dust deposition over the last 20,000 yr. *Earth and Planetary Science Letters*, *371*, 163-176.

Muschitiello, F., Zhang, Q., Sundqvist, H. S., Davies, F. J., & Renssen, H. (2015). Arctic climate response to the termination of the African Humid Period. *Quaternary Science Reviews*, *125*, 91-97.

Novello, V. F., Cruz, F. W., Vuille, M., Stríkis, N. M., Edwards, R. L., Cheng, H., ... & Santos, R. V. (2017). A high-resolution history of the South American Monsoon from Last Glacial Maximum to the Holocene. *Scientific reports*, *7*(1), 1-8.

Otto-Bliesner, B. L., Braconnot, P., Harrison, S. P., Lunt, D. J., Abe-Ouchi, A., Albani, S., ... & Zhang, Q. (2017). The PMIP4 contribution to CMIP6–Part 2: Two interglacials, scientific objective and experimental design for Holocene and Last Interglacial simulations. *Geoscientific Model Development*, *10*(11), 3979-4003.

Palchan, D., & Torfstein, A. (2019). A drop in Sahara dust fluxes records the northern limits of the African Humid Period. *Nature communications*, *10*(1), 1-9.

Pausata, F. S., Messori, G., & Zhang, Q. (2016). Impacts of dust reduction on the northward expansion of the African monsoon during the Green Sahara period. *Earth and Planetary Science Letters*, *434*, 298-307.

Pausata, F. S., Zhang, Q., Muschitiello, F., Lu, Z., Chafik, L., Niedermeyer, E. M., ... & Liu, Z. (2017). Greening of the Sahara suppressed ENSO activity during the mid-Holocene. *Nature communications*, *8*(1), 1-12.

Pausata, F. S., Emanuel, K. A., Chiacchio, M., Diro, G. T., Zhang, Q., Sushama, L., ... & Donnelly, J. P. (2017). Tropical cyclone activity enhanced by Sahara greening and reduced dust emissions during the African Humid Period. *Proceedings of the National Academy of Sciences*, *114*(24), 6221-6226.

Pausata, F. S., Gaetani, M., Messori, G., Berg, A., de Souza, D. M., Sage, R. F., & DeMenocal, P. B. (2020). The greening of the Sahara: Past changes and future implications. *One Earth*, *2*(3), 235-250.

Peltier, W. R., & Vettoretti, G. (2014). Dansgaard-Oeschger oscillations predicted in a comprehensive model of glacial climate: A "kicked" salt oscillator in the Atlantic. *Geophysical Research Letters*, *41*(20), 7306-7313.

Piao, J., Chen, W., Wang, L., Pausata, F. S., & Zhang, Q. (2020). Northward extension of the East Asian summer monsoon during the mid-Holocene. *Global and Planetary Change*, *184*, 103046.

Prado, L. F., Wainer, I., & Chiessi, C. M. (2013). Mid-Holocene PMIP3/CMIP5 model results: Intercomparison for the South American monsoon system. *The Holocene*, *23*(12), 1915-1920.

Rachmayani, R., Prange, M., & Schulz, M. (2015). North African vegetation–precipitation feedback in early and mid-Holocene climate simulations with CCSM3-DGVM. *Climate of the Past*, *11*(2), 175-185.

Schneider, U., Becker, A., Finger, P., Meyer-Christoffer, A., Rudolf, B., & Ziese, M. (2011). GPCC full data reanalysis version 6.0 at 0.5: Monthly land-surface precipitation from rain-gauges built on GTS-based and historic data. *GPCC Data Rep., doi*, *10*, 585.

Sha, L., Ait Brahim, Y., Wassenburg, J. A., Yin, J., Peros, M., Cruz, F. W., ... & Cheng, H. (2019). How far north did the African monsoon fringe expand during the African humid period? Insights from Southwest Moroccan speleothems. *Geophysical Research Letters*, *46*(23), 14093-14102.

Shanahan, T. M., McKay, N. P., Hughen, K. A., Overpeck, J. T., Otto-Bliesner, B., Heil, C. W., ... & Peck, J. (2015). The time-transgressive termination of the African Humid Period. *Nature Geoscience*, *8*(2), 140-144.

Shimizu, M. H., Sampaio, G., Venancio, I. M., & Maksic, J. (2020). Seasonal changes of the South American monsoon system during the Mid-Holocene in the CMIP5 simulations. *Climate Dynamics*, *54*(5), 2697-2712.

Silva Dias, P. L., Turcq, B., Silva Dias, M. A. F., Braconnot, P., & Jorgetti, T. (2009). Mid-Holocene climate of tropical South America: a model-data approach. In *Past climate variability in South America and surrounding regions* (pp. 259-281). Springer, Dordrecht.

Sun, W., Wang, B., Zhang, Q., Pausata, F. S., Chen, D., Lu, G., ... & Liu, J. (2019). Northern Hemisphere land monsoon precipitation increased by the Green Sahara during Middle Holocene. *Geophysical Research Letters*, *46*(16), 9870-9879.

Tabor, C., Otto-Bliesner, B., & Liu, Z. (2020). Speleothems of South American and Asian monsoons influenced by a Green Sahara. *Geophysical Research Letters*, *47*(22), e2020GL089695.

Thompson, A. J., Tabor, C. R., Poulsen, C. J., & Skinner, C. B. (2021). Water isotopic constraints on the enhancement of the mid-Holocene West African monsoon. *Earth and Planetary Science Letters*, *554*, 116677.

Tierney, J. E., Lewis, S. C., Cook, B. I., LeGrande, A. N., & Schmidt, G. A. (2011). Model, proxy and isotopic perspectives on the East African Humid Period. *Earth and Planetary Science Letters*, *307*(1-2), 103-112.

Tierney, J. E., Lewis, S. C., Cook, B. I., LeGrande, A. N., & Schmidt, G. A. (2011). Model, proxy and isotopic perspectives on the East African Humid Period. *Earth and Planetary Science Letters*, *307*(1-2), 103-112.

Wang, X., Edwards, R. L., Auler, A. S., Cheng, H., Kong, X., Wang, Y., ... & Chiang, H. W. (2017). Hydroclimate changes across the Amazon lowlands over the past 45,000 years. *Nature*, *541*(7636), 204-207.

Watrin, J., Lézine, A. M., & Hély, C. (2009). Plant migration and plant communities at the time of the “green Sahara”. *Comptes Rendus Geoscience*, *341*(8-9), 656-670.

Geophysical Research Letters

Supporting Information for

On the remote impacts of mid-Holocene Saharan vegetation on South American hydroclimate: a modelling intercomparison

S. Tiwari[1], R. D. Ramos[2], F. S. R. Pausata[1], A. N. LeGrande[3,4], M. L. Griffiths[2], H. Beltrami[5], I. Wainer[6], A. de Vernal[1], D. T. Litchmore[4,3], D. Chandan[7], W. R. Peltier[7], and C. R. Tabor[8]

[1]Centre ESCER (Étude et la Simulation du Climat à l'Échelle Régionale) and GEOTOP (Research Center on the dynamics of the Earth System), Department of Earth and Atmospheric Sciences, University of Quebec in Montreal, Montreal, Canada.

[2]Department of Environmental Science, William Paterson University, Wayne, New Jersey, USA.

[3]NASA Goddard Institute for Space Studies, New York, New York, USA.

[4]Center for Climate Systems Research, Columbia University, New York, New York, USA.

[5]Department of Earth Sciences, St. Francis Xavier University, Antigonish, Nova Scotia, Canada.

[6]Departamento de Oceanografia Física, Química e Geológica, Instituto Oceanográfico da Universidade de São Paulo, Praça do Oceanográfico, Sao Paulo, Brazil.

[7]Department of Physics, University of Toronto, Toronto, Ontario, Canada.

[8]Department of Geosciences, University of Connecticut, Storrs, Connecticut, USA.

Contents of this file

Text S1.

Model evaluations

A comparison of the model pre-Industrial simulations with observational and reanalysis datasets indicates that overall, the models faithfully capture the large-scale patterns of precipitation, though there are some model-specific regional biases (Fig. S2). For example, there is an overestimation of precipitation in northwestern Amazon region in UofT-CCSM4 and an under-estimation of precipitation in northern South America in iCESM 1.2. To different extents, some shortcomings are common to all models. These include: (i) a double-ITCZ and (ii) an under-estimation of precipitation over the southwestern South Atlantic Ocean. However, all models show reasonable magnitudes and distributions of annual precipitation, especially over the domain of the West African Monsoon, the Inter Tropical Convergence Zone and the South Atlantic Convergence Zone.

Text S2.

Representation of the mid-Holocene Green Sahara (MH_{GS}) in the models

The mid-Holocene (MH) was characterized by large-scale vegetation changes from desert to shrub and savanna over northern Africa. The PMIP4 recommendations for vegetation sensitivity experiments include changing vegetation over the Sahara to evergreen shrub up to 25 °N and savanna/steppe vegetation poleward of 25 °N (Otto-Bliesner et al., 2017). The vegetation changes also led to decreases in dust mobilization and soil albedo, and changes in surface hydrology.

Different models in this study treat the presence of the Green Sahara differently. In the EC-Earth 3.1 MH_{GS} simulation, vegetation over the Sahara was set to shrub, and dust was reduced by up to 80% relative to the PI. In the iCESM 1.2 MH_{GS} simulation, present day Sahelian land surface and vegetation characteristics at 11 °N were imposed over the Sahara. The use of an interactive dust scheme led to a decrease in dust mobilization. In the UofT-CCSM4 MH_{GS} simulation, tropical rainforests were extended northwards, the Sahara was completely replaced by evergreen shrubs up to 25 °N and almost completely (90%) replaced by a mix of steppe and savanna beyond 25 °N. Further, soil albedo was reduced to reflect greater moisture and organic matter, and the presence of five megalakes was incorporated through land surface changes. In the GISS-E2.1-G MH_{GS} simulation, bare soil and grass over the Sahara were replaced by arid shrub below 25 °N and by grassland above 25 °N.

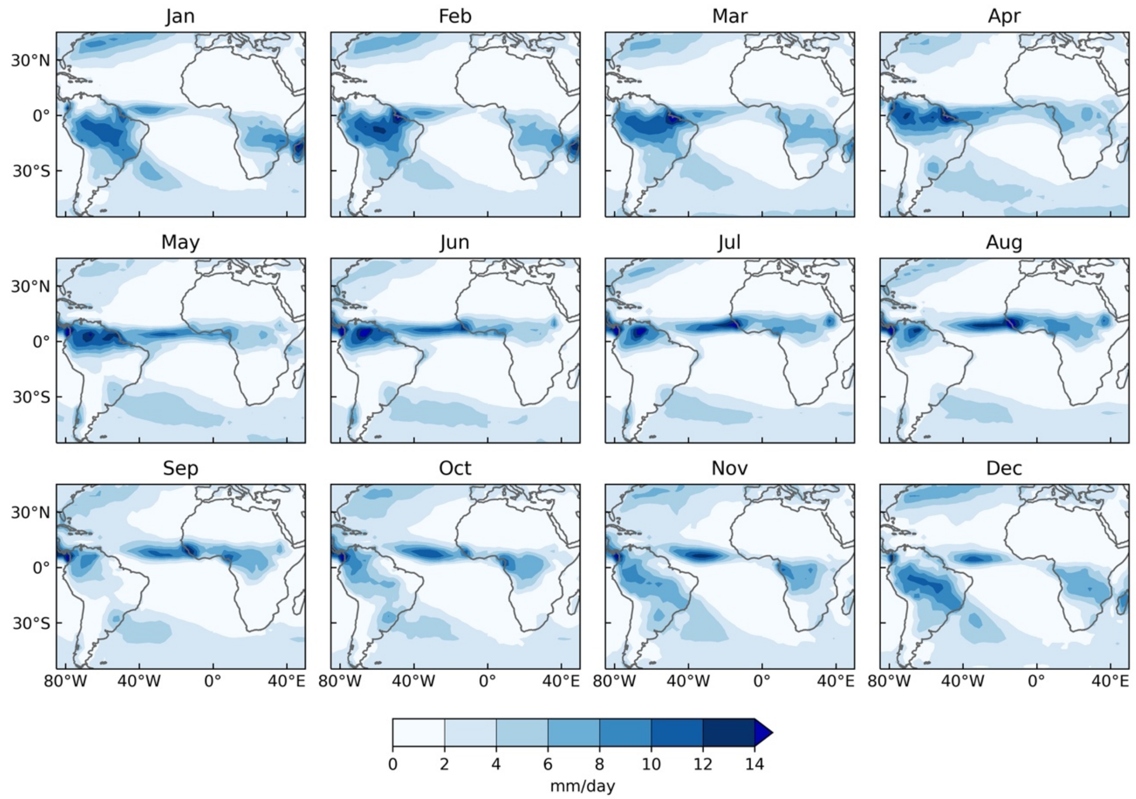

Figure S1. Present-day monthly precipitation patterns from the Global Precipitation Climatology Project (GPCP) version 2.2 from 1979-2009 (Huffman et al., 2015).

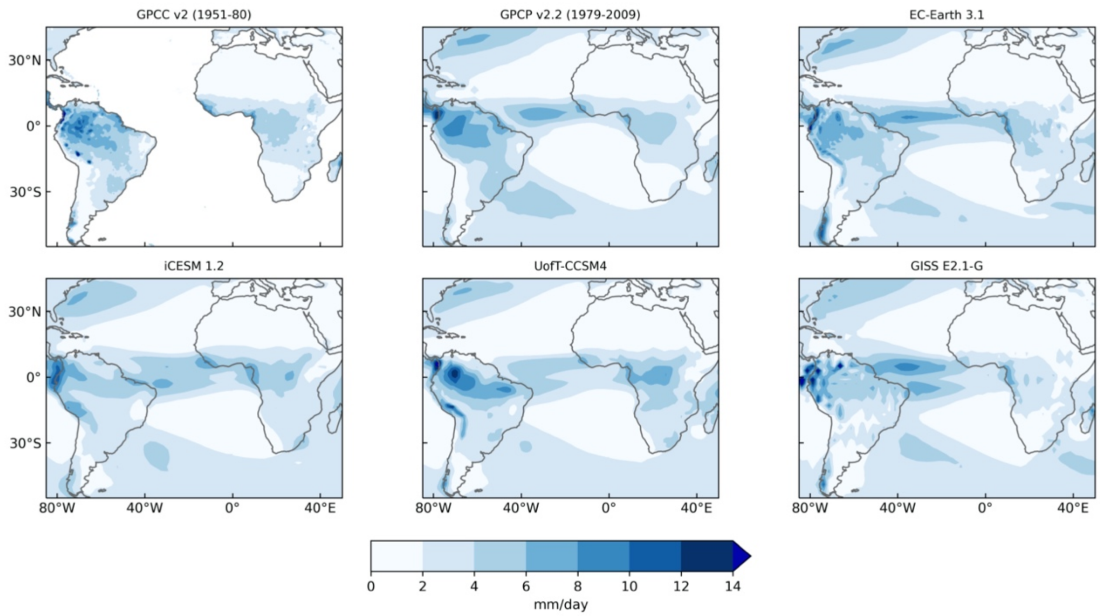

Figure S2. Comparison of annual precipitation patterns over South America between the Global Precipitation Climatology Centre (GPCC) Reanalysis Dataset, Global Precipitation

Climatology Project (GPCP) Dataset and the PI simulations from EC-Earth 3.1, iCESM 1.2, UofT-CCSM4 and GISS-E2.1-G.

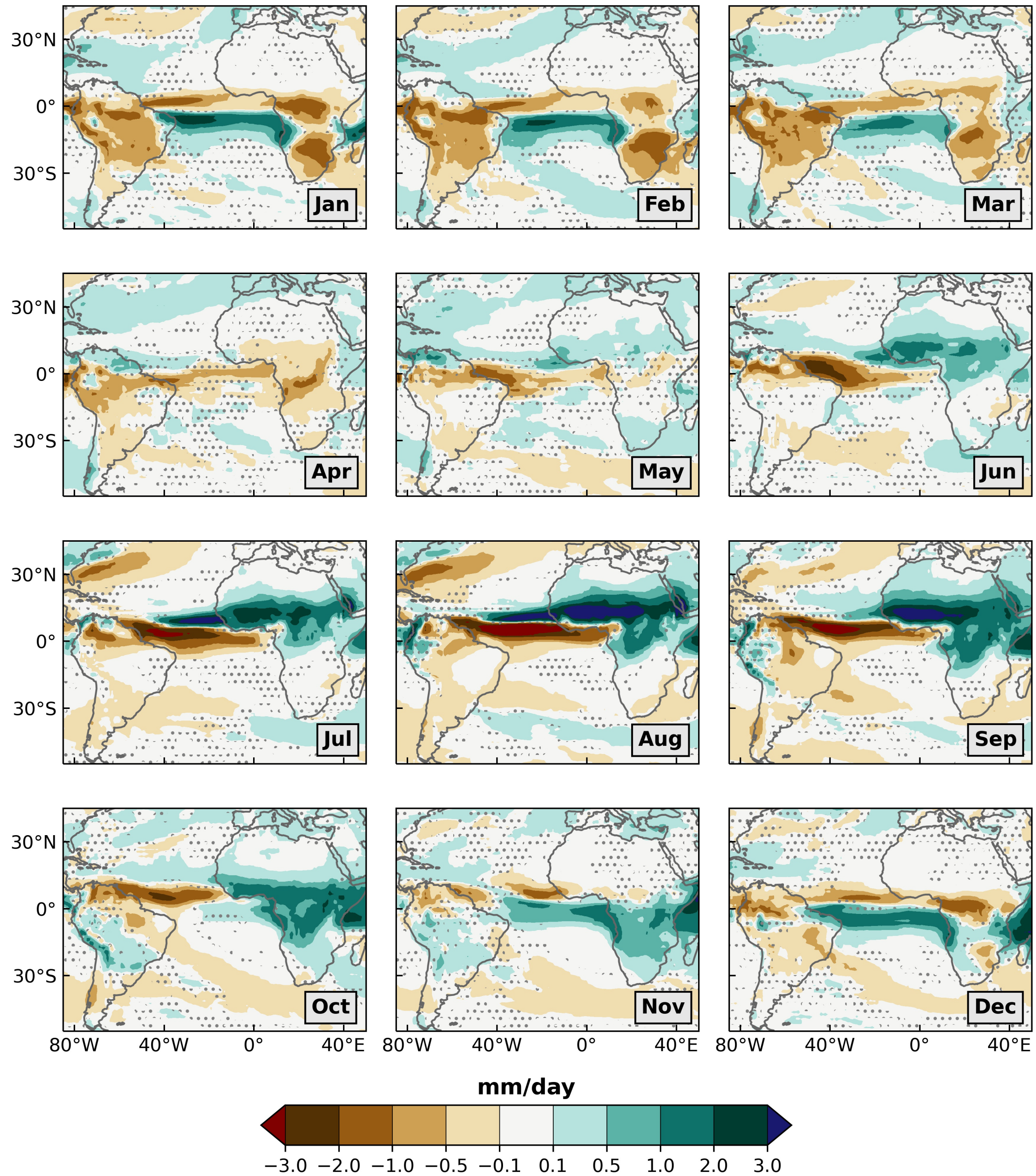

Figure S3. Precipitation changes between MH_{PMIP} and PI experiments, shown as multi-model averages for each month. Areas in which less than three models agree on the sign change are hatched.

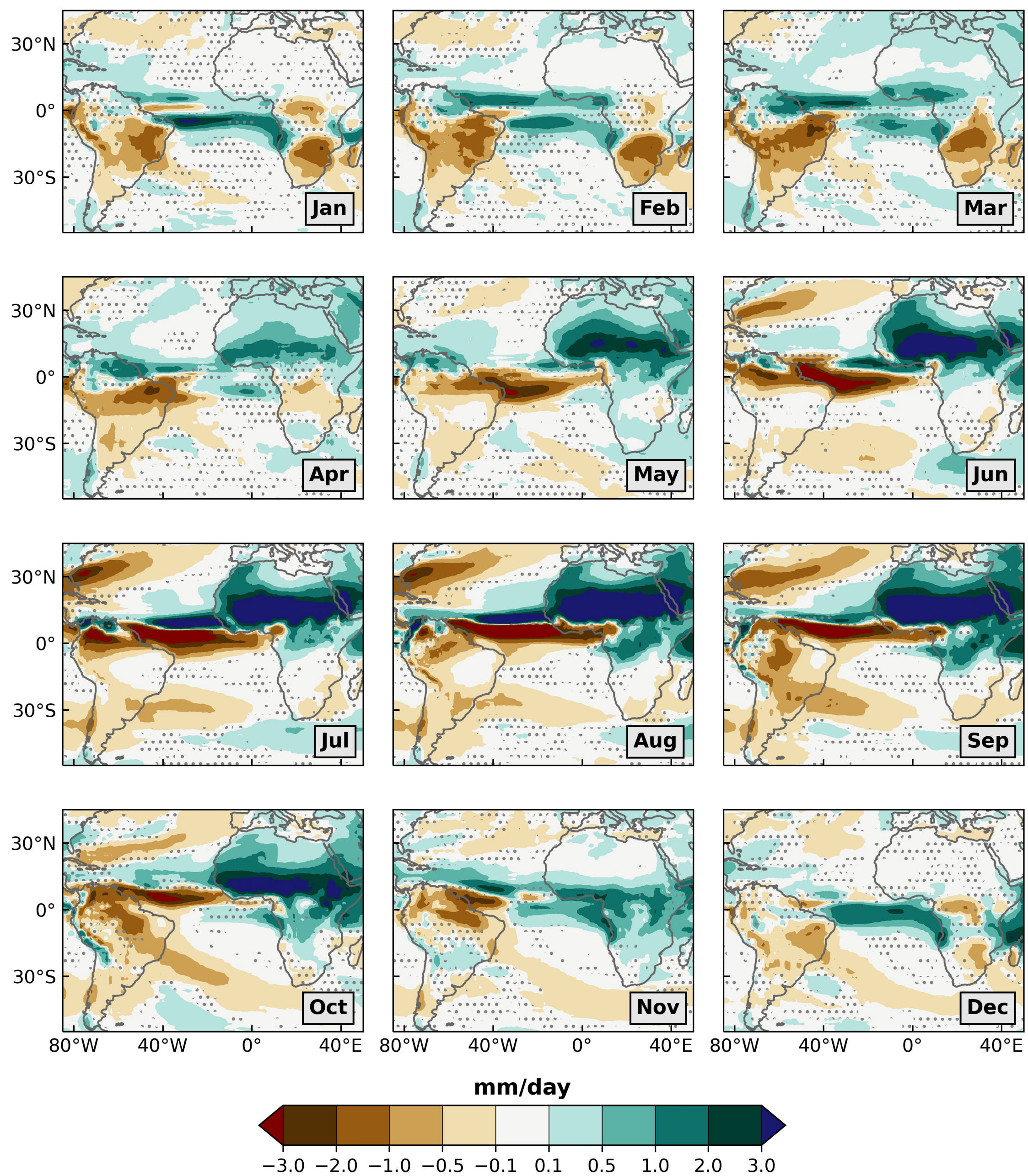

Figure S4. Precipitation changes between MH_{GS} and PI scenarios, shown as multi-model averages for each month. Areas in which less than three models agree on the sign change are hatched.

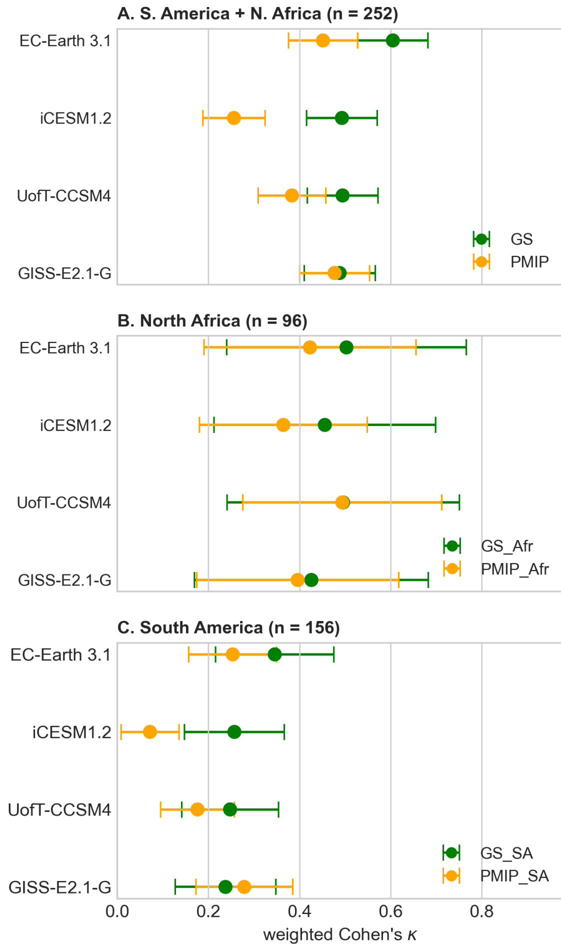

Figure S5. Weighted Cohen's k score between MH_{GS} (blue dots) and MH_{PMIP} (orange dots) scenarios over (a) South America and northern Africa, (b) northern Africa (0° to 38°N and 20°W to 45°E) and (c) South America (50°S to 15°N and 80°W to 30°W) regions. All datapoints are statistically significant ($p < 0.05$). Error bars indicate 95% confidence intervals.

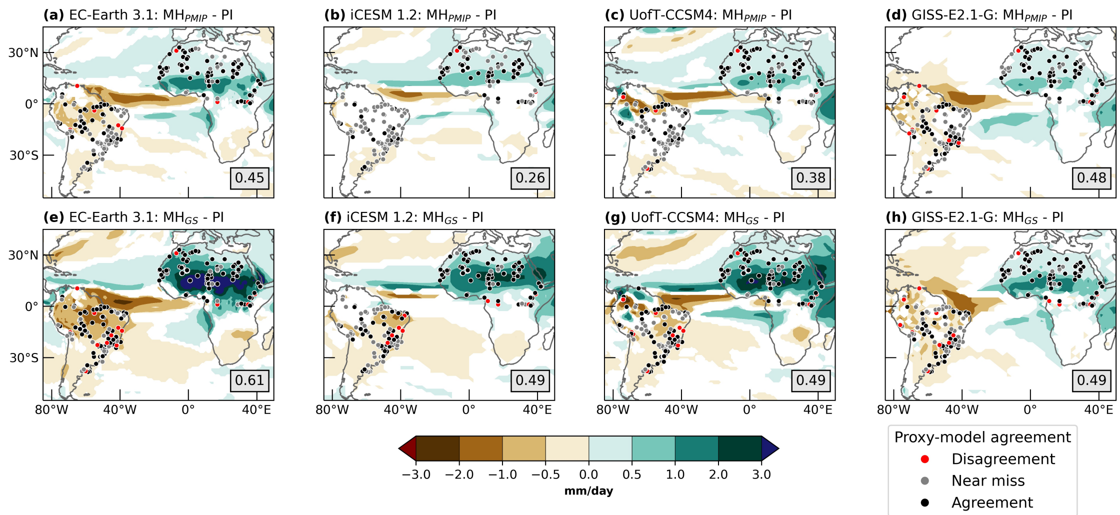

Figure S6. Proxy-model agreement over the region of study. Colors show MH-PI annual precipitation changes in mm/day. Only changes significant at the 95% confidence level are shown. Proxy sites are shown by circles, with the color indicating disagreement ("total miss"; red), near-miss (grey) and agreement (black).

	EC-Earth 3.1	**iCESM 1.2**	**UofT-CCSM4**	**GISS-E2.1-G**
Model name	EC-Earth	Community Earth System Model	Community Climate System Model	Goddard Institute for Space Studies Model
Atmospheric component	Integrated Forecast System	Community Atmosphere Model v5.3 (iCAM5)	Community Atmosphere Model v4 (CAM4)	Goddard Institute for Space Studies Model E2.1
Atmospheric grid	1.125 x 1.125 (62)	1.9 x 2.5 (30)	1 x 1 (26)	2 x 2.5 (40)
Oceanic component	Nucleus for European Modelling of the Ocean v2 (NEMO2)	Parallel Ocean Program v2.0 (POP2)	Parallel Ocean Program v2.0 (POP2)	GISS Ocean Model v1
Oceanic grid	1 x 1 (46)	1 x 1 (60)	1 x 1 (60)	1 x 1.25 (40)
Simulation protocols	CMIP5 / PMIP3	CMIP6 / PMIP4	CMIP6 / PMIP4	CMIP6 / PMIP4
Feedbacks incorporated in the MH_{GS} simulation	Vegetation, dust	Vegetation, dust, soil	Vegetation, soil, lakes	Vegetation
PI-to-MH albedo change over northern Africa	0.3 to 0.15	0.3 to 0.15	0.3 to 0.16	0.3 to 0.19
Reference for simulations	Pausata et al. (2016)	Tabor et al. (2020)	Chandan and Peltier (2020)	This paper

Table S1. Model details. Numbers in parentheses indicate number of vertical levels in the atmospheric or oceanic grid.